EurJOC
European Journal of Organic Chemistry

Research Article
doi.org/10.1002/ejoc.202300168

Chemistry Europe
European Chemical Societies Publishing

www.eurjoc.org

Special Collection

Synthesis, Structural Characterization, and Reductive Cleavage of an Oxygen-Containing Naphthyl Macrocycle

Zheng Zhou,[a, b] Matthew Pennachio,[a] Zheng Wei,[a] Maxi L. Heldner,[c] Marina A. Petrukhina,*[a] and Tobias A. Schaub[+]*[c]

Tobias A. Schaub was nominated to be part of this collection by EurJOC Board Member Oliver Dumele

A small macrocycle comprising ether-bridged naphthyl units was prepared in a two-step synthesis. Single-crystal X-ray diffraction of two polymorphs are reported, one of which showed multiple C–H···$\pi_{naphthyl}$ interactions of a solvent molecule in the cavity of the macrocycle. Chemical reduction led to C–O bond cleavages accompanied by a *Z*/*E* isomerization. The resulting twofold negatively charged (*E*)-1,2-bis(2-naphthyl)ethylene fragment was isolated as its potassium salts. Electronic characterization revealed a singlet ground state, and a marked distortion of the central ethylene unit was observed upon electron uptake.

Introduction

With the pioneering work on cyclic polyethers conducted by Pedersen in 1967,[1] macrocyclic chemistry has developed into a thriving field of research with implications for research all the way to practical applications.[2,3] Paradigmatic classes of artificial macrocycles that have received increased attention from the scientific community in the last decade include cycloparaphenylenes,[4] cucurbiturils,[5] calixarenes,[6] pillararenes,[7] as well as a plethora of cyclophanes,[8] to name a few. Many of these compounds own their popularity to a varying degree of flexible adaptive behaviour and shape persistence paired with the opportunity to tune these inherent properties by bottom up synthetic approaches.[9] Shape complementarity is often exploited in order to achieve remarkably high association constants in host guest complexes – the tight binding of fullerene C_{60} in [10]CPP with $K_a = 2.79 \pm 0.03 \times 10^6$ mol L^{-1} may serve as a paradigmatic example here.[10] Studies on ring currents and charge delocalization phenomena in phenylene based macrocycles have revealed a stabilizing effect for many negatively[11–13] and positively charged derivatives[14] due to global aromaticity while local aromatic ring currents often prevail in the neutral state.[15] In line with this observation, the groups of Choi and Glöcklhofer have recently rediscovered poly(*p*-phenylene vinylene)s based macrocycles as potent battery electrode material with excellent redox properties and charge storage performances by switching between a local aromatic and a global aromatic state.[16] While property tuning in these phenylene based macrocycles has been achieved by attachment of suitable for example electroactive or chromophoric substituents without changing the macrocycle shape to a large extent,[17] incorporation of for example heteroatoms into the backbone has direct consequences for the conjugation, the geometry, and the chemical stability of the macrocycle.[3] In this work, we report on the preparation and structural characterization of a conceptually simple macrocycle comprising (*Z*)-bis(2-naphthyl)ethylene units and ether bridges. Our main motivation was to study this compound in its negatively charged state and evaluate a potential stabilizing effect of its macrocyclic nature preventing the reported cleavage of linear aryl ethers under strongly reductive conditions.[18] While the studied macrocycle did not afford stable chemically reduced species under the conditions used, we were able to identify the main decomposition product – a doubly reduced (*E*)-bis(2-naphthyl)ethylene – resulting from a multistage fragmentation/isomerization reaction. The dianion was investigated by joint X-ray crystallographic structure determination, NMR and UV-vis spectroscopy and computational elucidation of the electronic structure.

[a] Dr. Z. Zhou, M. Pennachio, Dr. Z. Wei, Prof. Dr. M. A. Petrukhina
Department of Chemistry
University at Albany
State University of New York
1400 Washington Avenue, Albany, NY 12222 (USA)
E-mail: mpetrukhina@albany.edu
[b] Dr. Z. Zhou
School of Materials Science and Engineering
Tongji University
4800 Cao'an Road, Shanghai 201804 (P. R. China)
[c] M. L. Heldner, Dr. T. A. Schaub[+]
Institute of Organic Chemistry
Ruprecht-Karls-University Heidelberg
Im Neuenheimer Feld 270, 69120 Heidelberg (Germany)
E-mail: Tobias.schaub@uni-heidelberg.de

[+] *Tobias A. Schaub was nominated to be part of this collection by EurJOC Board Member Oliver Dumele.*

Supporting information for this article is available on the WWW under https://doi.org/10.1002/ejoc.202300168

Special Collection *Part of the*

Research Article
doi.org/10.1002/ejoc.202300168

Results and Discussion

Macrocycle **3** was available by performing three synthetic steps starting from commercially available 6-bromo-2-naphthol (Figure 1, for details see the Supporting Information). Briefly, following the protocol reported by Yamaguchi et al.[19] an acid-catalyzed condensation gave the symmetrical, substituted naphthyl ether **1**, which was further converted to bisaldehyde **2** via a sequential lithiation/formylation path. The macrocyclizative dimerization under standard McMurry conditions reported by Grützmacher et al.[20] was conducted under pseudo high dilution conditions in which **2** (0.1 M) was slowly added to a Ti^0 solution (0.06 M) within 5 h (for details see the experimental section). The reaction afforded the target compound after chromatographic purification in 20% yield. Quick et al.[21] observed a *Z*/*E* ratio of 0.60:0.40 when dimerizing 2-naphthaldehyde which most likely accounts for the low to moderate yield, since initial *E*-ethylene formation prevents subsequent macrocyclization.

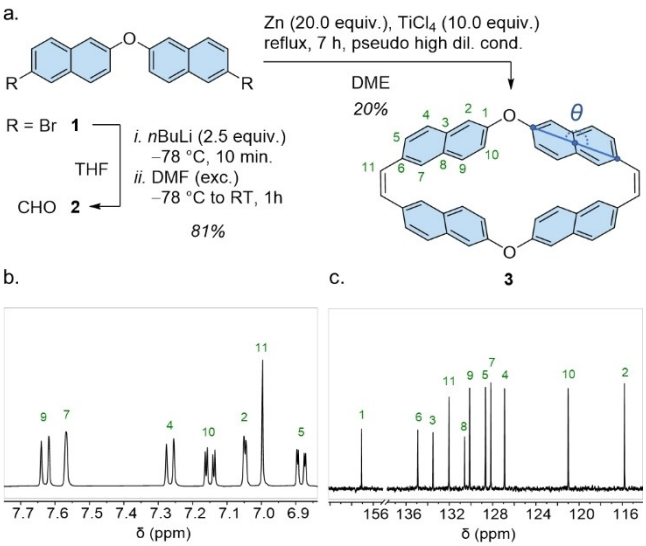

Figure 1. Synthesis of **3** and definition of naphthyl bending angle θ (a), ^1H (400.1 MHz, b), and ^{13}C NMR characterization (100.7 MHz, CD_2Cl_2, r.t., c) together with the peak assignment; for details see the Supporting Information.

Compound **3** is a colourless microcrystalline substance with good solubility in polar and chlorinated organic solvents such as THF and CH_2Cl_2. Variable temperature ^1H NMR spectrum of **3** shows six unique signals characteristic for a 2,6-disubstituted naphthyl unit without considerable conformational restrictions due to macrocyclic ring strain even at low temperatures ($T = -30\,°C$, see the Supporting Information, Figure S21). In other words, compound **3** is conformationally fluxional via facile rotation of naphthyl units about their 2,6-axis.

By slow evaporation of **3** in toluene, a solvated polymorph, $C_{44}H_{28}O_2{\cdot}C_7H_8$ (**3-t**, 't' stands for toluene), was isolated (Figure 2a,b). The crystal structure of **3-t** reveals the internal space of the macrocycle is capable of accommodating a methylene unit from a toluene molecule, with multiple C–H···π contacts ranging from 2.688(8) to 2.739(8) Å (see the Supporting Information, Figure S36). In the solid-state structure of **3-t**, a 3D

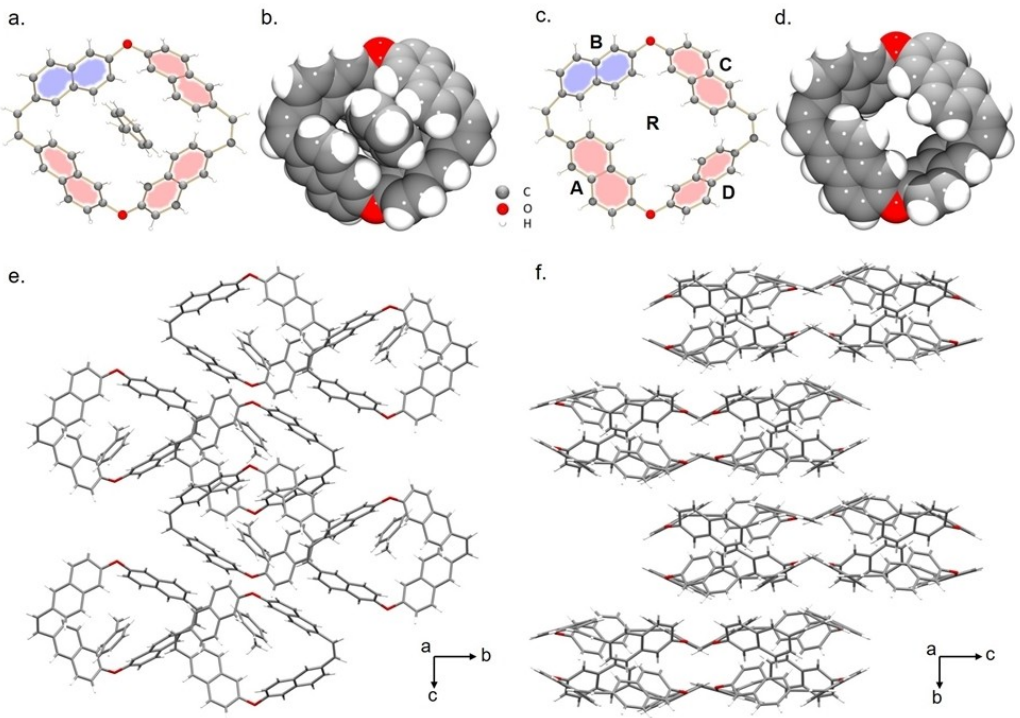

Figure 2. Crystal structures of **3-t** (red/blue color denote naphthyl rings of different symmetry; a, b;) and **3-u** (c,d) in ball-and-stick and space-filling models, and solid state packing of **3-t** (e) and **3-u** (f) in capped-stick models.

Research Article
doi.org/10.1002/ejoc.202300168

network is formed through relatively strong C–H···π interactions between adjacent molecules, with shortest distances ranging from 2.602(8) to 2.731(8) Å (Figure 2e). In contrast, sublimation of **3** at 280 °C in an evacuated glass ampule for five days afforded colourless blocks (yield ca. 85 %), which were confirmed to be a solvent-free polymorph (**3-u**, 'u' stands for unsolvated, Figure 2c,d). In the solid-state structure of **3-u**, a 3D network is formed through a combination of C–H···π and π···π interactions between adjacent molecules, with the distances of 2.543(2)–2.722(2) Å and 3.121(2) Å, respectively (Figure 2f). The direct comparison of the macrocycle geometry in **3-t** and **3-u** is informative. Due to guest solvent entrapment, the dihedral angles between naphthyl rings and the central plane R in **3-t** (avg. 45.6°, Table S2) and the internal space (ca. 164 Å^3) are relatively large (Figure S39). In contrast, a distinctive decrease of A/R (27.0°) and C/R (19.6°) angles along with shrinking of the internal space (ca. 95 Å^3), are observed in **3-u**. While having an inner cavity size similar to [6]CPP,[22] notable core flexibility of the macrocycle is illustrated by the formation of the two different polymorphs and the free rotation of the naphthyl backbone units observed in the ^{1}H NMR spectrum. For both polymorphs, compound **3** adopts a non-symmetric geometry with one naphthyl unit flipped along the 2,6-disubstitution axis (see Figure 2 blue ring fill colour).

To understand the preference of this particular molecular conformation we calculated a conformer library of **3** using density functional theory (DFT, B97D3/def2-TZVP, gas phase, for details see the Supporting Information, Figure S42) and validated our geometry predictions by comparison to the solid-state structure (RMSD is 0.091 Å for the shown conformer of **3**). We find a weak macrocyclic ring strain of +2.9 kcal/mol which is structurally reflected in a slight bending of the naphthyl rings around a bending angle θ (for definition of θ see Figure 1a, for homodesmotic reactions see the Supporting Information, Scheme S1); the average bending is slightly larger in the experimentally obtained structures ($\theta = 173.9°$ for **3-u** and 175.2° for **3-t**) than in the corresponding computationally predicted conformer **3 c** ($\theta = 175.5°$). The experimentally observed conformation of **3** is higher in energy by about +1.3 kcal/mol compared to the thermodynamically most stable conformer in which opposing naphthyl groups have the same orientation. We ascribe this observation to packing effects, i.e. mostly π···π interactions, which are known to be able to compensate for energetic drawbacks.[23] As a matter of fact, a closer look at the crystal structure reveals a second conformer for both structures **3-u** and **3-t** with split occupancy (ratio **3-u/3-u'** 0.89:0.11, ratio **3-t/3-t'** 0.60:0.40) in which all naphthyls exhibit the same orientation ($\Delta E = +1.6$ kcal mol^{-1}, see the Supporting Information, Table S6). These results are in good agreement with the observed fast interconversion of conformers at room temperature (see above).

With the goal of investigating the ability of **3** to accommodate multiple electrons via chemical reduction we treated the macrocycle with excess K metal in THF at room temperature (Figure 3). The reaction proceeds through a blue-green followed by a dark purple colour within less than 60 min, which is

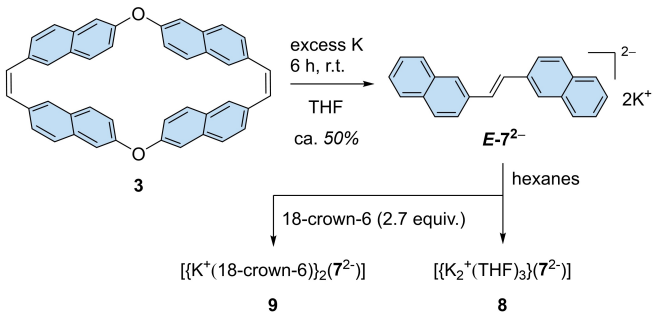

Figure 3. Reductive cleavage of macrocycle **3** with K metal in THF.

indicative of a two-step reduction process (for further details on the UV-Vis absorption traces see the Supporting Information).

By slow diffusion of hexanes into the purple THF solution, the main product was isolated as small dark blocks in ca. 50 % yield after 1 month. Single crystal X-ray diffraction confirmed the formation of a contact-ion product of the composition [{K_2^+(THF)$_3$}($C_{22}H_{16}^{2-}$)] (**8**). When 18-crown-6 ether was used as the secondary ligand during crystallization, small dark plates were isolated, which were identified by X-ray diffraction as [{K^+(18-crown-6)}$_2$($C_{22}H_{16}^{2-}$)] (**9**). Notably, in both crystal structures, the macrocycle has been cleaved upon chemical reduction to a new chain fragment, namely the $C_{22}H_{16}^{2-}$ anion in *E* configuration (*E*-**7**$^{2-}$). Similar irreversible reductions of macrocyclic aryl ethers have been observed by *Neumüller* and co-workers using cyclic voltammetry.[24]

Accurate analysis of rather the large amounts of side products was challenging due to the complex nature of the mixture. Nevertheless, insight was gained by treating a freshly prepared solution of **3** with elemental potassium and quenching the resulting dark purple solution after two hours by addition to a mixture of *i*PrOH in THF. GC-MS analysis of the crude reaction mixture suggested formation of **7**$^{2-}$ (relative yield ca. 41 %) together with the corresponding mono- (ca. 12 %) and bisalcohol cleavage product (ca. 22 %) as the main species (see Figure S30, Supporting Information). In contrast, subjecting di-2-naphthylether to equal reaction conditions revealed a rather clean ether cleavage after quenching with *i*PrOH/THF to yield naphthalene/2-naphthol in a ratio of ca. 0.49:0.51 as the main products (see Figure S25, Supporting Information) which led us to conclude that the alkene unit as well participates in decomposition reactions. Considering the small reaction scale, we assume that trace amounts of water present in THF significantly affect the reaction path by rapid protonation of reduced species at the alkene unit. Proof came from a computational study of 2,2'-dinapthylstilbene dianion *E*-**7**$^{2-}$ showing a significant accumulation of charge at the central C=C double bond (see below) as well as two control experiments; To this end, a solution of **7**$^{2-}$ was prepared by stirring (*Z*)-1,2-bis(2-naphthyl)ethylene with excessive potassium in THF for two hours and subsequent quenching by *i*) addition to *i*PrOH/THF or *ii*) to excessive iodine in THF. In the first case the crude product shows the corresponding 1,2-bis(2-naphthyl)ethane resulting from reduction and protonation of

Research Article
doi.org/10.1002/ejoc.202300168

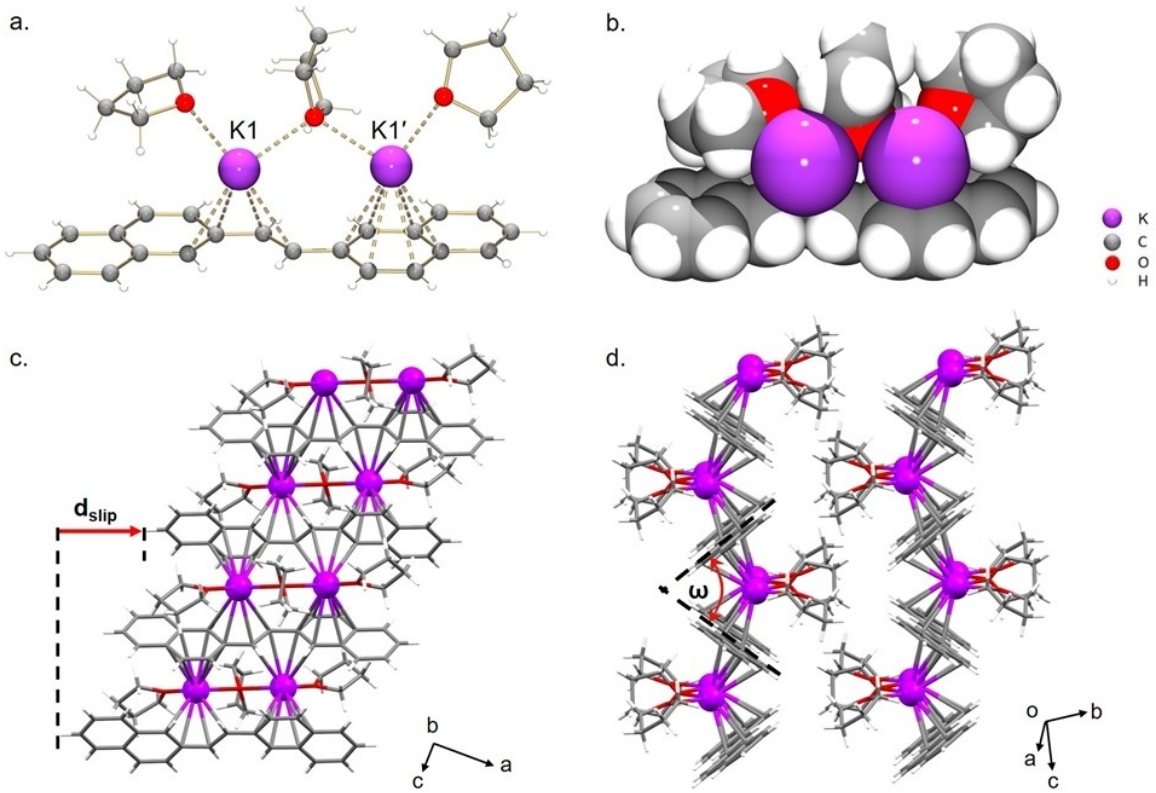

Figure 4. Crystal structure of **8** in ball-and-stick (a) and space-filling models (b), 1D column (c) and solid-state packing (d) in mixed models.

the alkene unit as the main product (Figure S28, Supporting Information). Quenching with I_2 in THF afforded a mixture of (*E*)-1,2- bis(2-naphthyl)ethylene and 1,2-bis(2-naphthyl)ethane in a ratio of 0.70:0.30 (Figure S29, Supporting Information), highlighting the sensitivity of this reaction to trace amounts of water present during the reaction.

In the crystal structure of **8** (Figure 4a,b), only one independent K^+ ion is found. The K^+ ion binds to the $\mathbf{7}^{2-}$ anions in the η^4- and η^6-modes (Figure S40), with the K–C distances of 3.007(2)–3.132(2) Å and 3.104(2)–3.159(2) Å, respectively (Table 1). The coordination environment of the K^+ ion is completed by one terminal and one shared THF molecules (K–O_{THF}: 2.722(7)– 2.742(1) Å). The K–C and K–O distances are analogous to those previously reported.[12,25–28] In the solid structure of **8**, the molecules are propagated into a 1D column along *c* axis through K–C coordination (Figure 4c). Notably, the $\mathbf{7}^{2-}$ anions are aligned in a herringbone pattern with the angle (ω) of 73.3° (Figure 4d), which is commonly seen in the alkali-metal intercalated acenes like anthracene and pentacene.[29] Moreover, the molecules are slipped in the column, with the slip distance (d_{slip}) of 7.47 Å. No further interactions are found between the adjacent columns.

Table 1. K–C distances (Å) in **8** and **9** along with the C-labelling schemes.

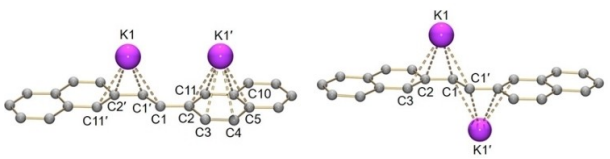

8 **9**

K1–C1	3.104(2)	K1–C10	3.166(2)	K1–C1	3.105(2)
K1–C2	3.128(2)	K1–C11	3.132(2)	K1–C2	3.188(2)
K1–C3	3.104(2)	K1–C1′	3.007(2)	K1–C3	3.295(2)
K1–C4	3.123(2)	K1–C2′	3.011(2)	K1–C1′	3.156(2)
K1–C5	3.160(2)	K1–C11′	3.109(2)		

In the crystal structure of **9** (Figure 5a,b), there is one independent K^+ ion entrapped by an axially bound 18-crown-6 molecule (K–O_{crown}: 2.722(7)–2.742(1) Å) (Table 1). Notably, the addition of 18-crown-6 breaks the 1D polymeric chain into the discrete species, accompanied by a change of metal coordination, that has been observed upon reduction of other PAHs.[26] The K^+ ion is η^4-coordinated to the center of the *E*-$\mathbf{7}^{2-}$ core with K–C distances of 3.105(2)–3.295(2) Å (Table 1). The K–C and K– O distances are comparable to those reported in the literature.[12,25–28] In the solid structure of **9**, a 2D layer is formed through C–H···π interactions (blue dotted lines) between the *E*-$\mathbf{7}^{2-}$ anions and the 18-crown-6 ether molecules (Figure 5c) with the distance measured at 2.729(4) Å.

It should be noted that the two-electron uptake leads to bond cleavage and hydrogenation of the naphthyl macrocycle (**3**). As a result, a new chain-like dianion $C_{22}H_{16}^{2-}$ (*E*-$\mathbf{7}^{2-}$) is formed in both **8** and **9** (Table 2 scheme). The $C_{22}H_{16}^{2-}$ core in both structures is planar, and the C–C bond alternation is

Research Article
doi.org/10.1002/ejoc.202300168

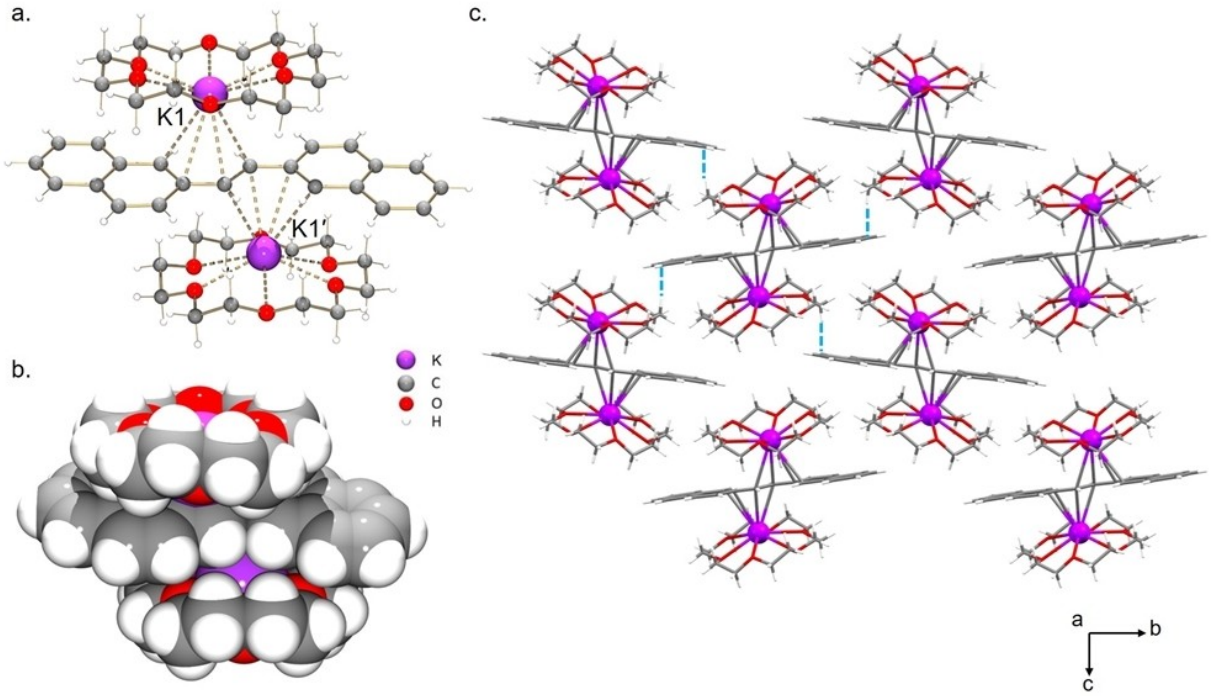

Figure 5. Crystal structure of **9** in ball-and-stick (a) and space-filling models (b), 1D column (c) and solid-state packing.

Table 2. Key C–C bond lengths (Å) and angles (°) of *E*-**7**$^{2-}$ in **8** and **9**, along with a labelling scheme in comparison to those in **3-u**; Values from geometry optimized structures (singlet electronic state, in blue).

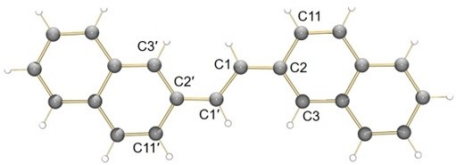

	3-u*	*E*-**7**	**8**	**9**
C1–C2	1.470(2)/1.471	1.458	1.405(3)	1.397(4)/1.417
C1–C1′	1.332(2)/1.350	1.351	1.427(3)	1.425(4)/1.427
C2–C3	1.413(2)/1.425	1.391	1.443(3)	1.431(4)/1.437
C2–C11	1.383(2)/1.387	1.428	1.437(3)	1.444(4)/1.440
C1′–C1–C2	127.3(2)/126.0	127.2	126.1(2)	126.1(2)/126.1

observed in the doubly-reduced products (Table 2). The C=C bond between two naphthyl units (C1–C1′) of 1.332(2) Å in **3-u** is elongated to 1.427(3) Å in **8** and 1.425(4) Å in **9**, respectively. In contrast, the C–C bonds adjacent to the C=C bond (C1–C2) are shortened from 1.470(2) Å to 1.405(3) Å in **8** and 1.397(4) Å in **9**, respectively. A similar trend was observed for the twofold reduction of dibenzo[*a*,*e*]cyclooctatetraene in which negative charge was localized at the central eight-membered ring.[26] It should be noted that the C=C bond is in *Z* configuration in **3-u** and is transformed to *E* configuration in **7**$^{2-}$ during the chemical reduction and ring-opening process.

Further insight into the electronic situation in the twofold reduced anion in **9** was provided by density functional theory (DFT) calculations at the B97D3/def2TZVP level of theory. The geometric distortions observed for structure **9** around the central alkene is reproduced in the geometry optimized structures (RMSD 0.054 Å for *E*-**7**$^{2-}$, see Table 2). In the gas phase the 2,2′-dinapthylstilbene dianion in **9** possesses a singlet electronic configuration in the ground state which is more stable by 13.1 kcal mol^{-1} than the corresponding triplet in agreement with well resolved signals in the ^{1}H NMR (see above, Figure S23). Our computational results indicate delocalization of the negative charges on the naphthyls with considerable charge accumulation on the central part of the 2,2′-dinapthylstilbene dianion *E*-**7**$^{2-}$ in **9**; the total Mulliken charge on the central fragment is −1.74e while the most pronounced increases in charge are seen for C1 (from −0.17e to −0.61e) and for C11 (from −0.32e to −0.60e, for further details see the Supporting Information). In general, the changes in bond lengths observed upon two-electron uptake are reflected by changes in Mayer's bond order, i.e. for C1–C1′ the bond order decreases from 1.68 to 1.13, accompanied by a lengthening of the bond from 1.351 Å to 1.427 Å upon reduction (for C1–C2: 1.08 to 1.14, 1.458 Å to 1.417 Å), C2–C3: 1.37 to 1.15, 1.391 Å to 1.437 Å; C2–C11: 1.17 to 1.10, 1.428 Å to 1.440 Å, see Table 2). In particular, the reduced bond order of C1=C1′ may account for the observed *Z*/*E* isomerization during chemical reduction. While a definitive deciphering of the underlying mechanism of this isomerization is beyond the scope of this study, early reports by Szwarc and co-workers[30] demonstrated the acceleration of the spontaneous *Z*/*E* conversion in the twofold negatively charged state of stilbene. Quite contrary, the intrinsic thermal isomerization of *Z*-stilbene radical anion was too slow to be observed directly, and a rate as low as 10^{-3} s^{-1} was extrapolated from kinetic analysis.[30] On the basis of these

Research Article
doi.org/10.1002/ejoc.202300168

previous results we suggest an involvement of the twofold negatively charged state in the isomerization to *E*-**7**$^{2-}$. Similarly our control experiments with (*Z*)-1,2-bis(2-naphthyl)ethylene (see Figure S29, see above) suggest accelerated *Z*/*E* isomerization in the reduced state.

Conclusion

In summary, we present a new macrocycle built from ether bridged (*Z*)-1,2-bis(2-naphthyl)ethylene units which can be prepared in a three-step synthesis using a McMurry macrocyclization strategy in the final step. The small macrocyclic ring strain leads to a minor bending of the naphthyl units from planarity which, however, were found to rotate along the 2,6-axis without considerable conformational restrictions. Interestingly, in one of the two reported polymorphs the methylene units of a toluene solvent molecule fills the cavity of the macrocycle by virtue of multiple C–H···π interactions suggesting potential for host/guest chemistry with small molecular entities. Under strongly reductive conditions multiple C–O bond cleavages and a *Z*/*E* isomerization lead to doubly reduced (*E*)-1,2-bis(2-naphthyl)ethylene which has been isolated as its potassium salts [{K$^+$(18-crown-6)}$_2$($C_{22}H_{16}^{2-}$)] and [{K_2^+(THF)$_3$}($C_{22}H_{16}^{2-}$)]. Structural and electronic characterization indicate a singlet ground state and marked distortion of the central ethylene unit was observed upon electron uptake. Based on our findings we suggest to avoid naphthyl ether bridges for the design of conjugated macrocycles if negatively charged species can be anticipated *in operando*.

Experimental Section

General. Unless otherwise noted, commercially available materials were used without purification. Moisture and oxygen sensitive reactions were carried out in flame-dried glassware and under an inert atmosphere of purified nitrogen using syringe/septa technique.

Macrocycle (3): A dried three neck flask equipped with a drip funnel and a reflux condenser was charged with zinc powder (5.60 g, 86.0 mmol, 20.0 equiv.) and dimethoxyethane (DME, anhydrous, 70 mL, 0.06 M) and cooled to 0 °C. Then $TiCl_4$ (8.2 g, 42.9 mmol, 10.0 equiv.) was added slowly via syringe and the mixture was heated at reflux for 1.5 h before bisaldehyde **2** (1.40 g, 4.29 mmol, 1.00 equiv.) in DME (42.0 mL, 0.1 M) was added dropwise within 5 h. After the addition was completed, the mixture was heated under reflux for another two hours and, then, allowed to cool to room temperature. The reaction was quenched by addition of sat. $NaHCO_3$ (50 mL) solution and extracted with ethyl acetate (4×30 mL). The organic layers were washed with water (30 mL) and brine (30 mL), dried over $MgSO_4$, and the solvent was removed under reduced pressure. Purification by column chromatography (SiO_2, 30–60 % CH_2Cl_2/*n*-hexane afforded product **3** as a colorless solid (250.00 mg, 0.42 mmol, 20 %). R_f (SiO_2, 66 % CH_2Cl_2/Hex) = 0.71; Mp. 297.7–298.4 °C. ^{1}H NMR (400 MHz, CD_2Cl_2): δ = 7.63 (d, J = 8.9 Hz, 2H, H-9), 7.57 (d, J = 1.9 Hz, 2H, H-7), 7.27 (d, J = 8.5 Hz, 2H, H-4), 7.15 (dd, J = 8.9, 2.5 Hz, 2H, H-10), 7.05 (d, J = 2.5 Hz, 2H, H-2), 7.00 (s, 4H, H-11), 6.88 ppm (dd, J = 8.5, 1.9 Hz, 1H, H-5); ^{13}C NMR (101 MHz, CD_2Cl_2): δ = 157.1 (C-1), 134.9 (C-6), 133.5 (C-3), 132.0 (C-1), 130.6 (C-8), 130.1 (C-9), 128.7 (C-5), 128.2 (C-7), 126.9 (C-4), 121.0 (C-10), 115.8 ppm (C-2); IR (ATR): $\tilde{\nu}$ = 3055 (w), 3011 (w), 1622 (w), 1595 (m), 1499 (w), 1466 (s), 1238 (s), 1200 (s), 1154 (s), 970 (m), 905 (s), 866 (s), 810 cm^{-1} (s); HRMS (MALDI, DCTB, positive) *m*/*z* calcd. for $C_{44}H_{28}O_2$ [M^+] 588.2084, found 588.2089.

Chemical Reduction: Materials and Methods: All manipulations were carried out using break-and-seal[31] and glove-box techniques under an atmosphere of argon. Tetrahydrofuran (THF) and hexanes (Sigma Aldrich) were dried over Na/benzophenone and distilled prior to use. THF-d_8 (99.95 atom % D, Sigma Aldrich) was dried over NaK_2 alloy and vacuum-transferred. Potassium (98 %) and 18-crown-6 ether (99 %) were purchased from Sigma Aldrich and used as received. The UV-Vis spectra were recorded on a Thermo Scientific Evolution 201 UV-Visible Spectrophotometer. The NMR spectra were measured on a Bruker Ascend-500 spectrometer at 500 MHz for ^{1}H and referenced to the resonances of THF-d_8. GC-MS (25–260 °C, 10 min, EI, He carrier gas) was carried out on a Shimadzu GCMS-QP2010 SE instrument.

[{K_2^+(THF)$_3$}(*E*-7**$^{2-}$)] (8)**: THF (1.3 mL) was added to a custom-built glass system containing **3** (4.0 mg, 0.007 mmol, sublimed at 280 °C) and excess K (5 mg, 0.128 mmol, 18 equiv.). The mixture was allowed to stir under argon at 25 °C for 6 h in a closed system. The initial off-white color (neutral ligand) of the suspension changed to turquoise after 2 min and deepened to purple after 10 min. The mixture was filtered through a sintered glass funnel, and the purple filtrate was layered with 3.0 mL of hexanes. The ampule was sealed and stored at −22 °C. Black blocks were present in solution after 1 month (2.0 mg, 50 %). ^{1}H NMR (500 MHz, THF-d_8, 25 °C): δ = 4.33–4.43 (2H, $C_{22}H_{16}^{2-}$), 5.22–5.31 (2H, $C_{22}H_{16}^{2-}$), 5.36–5.43 (2H, $C_{22}H_{16}^{2-}$), 5.47–5.55 (2H, $C_{22}H_{16}^{2-}$), 5.63–5.73 (2H, $C_{22}H_{16}^{2-}$), 5.78–5.90 (4H, $C_{22}H_{16}^{2-}$), 5.95–6.05 ppm (2H, $C_{22}H_{16}^{2-}$). UV-Vis (THF, nm): λ_{max} 378, 587.

[{K$^+$(18-crown-6)}$_2$(*E*-7**$^{2-}$)] (9)**: THF (1.5 mL) was added to a custom-built glass system containing **3** (2 mg, ca. 0.003 mmol, sublimed at 280 °C) and excess K (5 mg, 0.714 mmol, 36 equiv.). The mixture was allowed to stir under argon at 25 °C for 6 h in a closed system. The initial off-white color (neutral ligand) of the suspension changed to turquoise after 5 min and deepened to purple after 20 min. The mixture was filtered through a sintered glass funnel, and the purple filtrate was layered with 1.5 mL of hexanes containing 18-crown-6 (2 mg, 0.008 mmol). The ampule was sealed and stored at 5 °C. After 6 days, some black plates were present in solution (1.6 mg, 50 %).^{1}H NMR (500 MHz, THF-d_8, 25 °C): δ = 3.52–3.56 (24H, 18-crown-6), 4.37–4.41 (2H, $C_{22}H_{16}^{2-}$), 5.24–5.29 (2H, $C_{22}H_{16}^{2-}$), 5.37–5.42 (2H, $C_{22}H_{16}^{2-}$), 5.48–5.54 (2H, $C_{22}H_{16}^{2-}$), 5.67–5.72 (2H, $C_{22}H_{16}^{2-}$), 5.83–5.89 (4H, $C_{22}H_{16}^{2-}$), 5.97–6.04 ppm (2H, $C_{22}H_{16}^{2-}$). UV-Vis (THF, nm): λ_{max} 325.

Crystal Structure Solution and Refinement: Data collection of **3-t** was performed on a Bruker APEX-II Quazar diffractometer using $Mo_{K\alpha}$ radiation (λ = 0.71073 Å) at 200(2) K. Data collection of **8** was performed on a Bruker VENTURE system equipped with a PHOTON 100 CMOS detector, a Mo-target fine-focus X-ray source (λ = 0.71073 Å), and a graphite monochromator. The data were collected at 100(2) K (Oxford Cryosystems CRYOSTREAM 700), 50 kV, and 30 mA with an appropriate 0.5° ω scan strategy. The single crystal diffraction data for **3-u** and **9** were measured on a Bruker D8 VENTURE X-ray diffractometer equipped with a PHOTON 100 CMOS shutterless mode detector and an INCOATEC IμS micro-focus Cu-target X-ray tube (λ = 1.54178 Å) at T = 100(2) K. Data were collected using both ϕ and ω scans. All data sets' reduction and integration were performed with the Bruker software package SAINT (version 8.38 A).[32] Data were corrected for absorption effects using the empirical methods as implemented in SADABS (version 2016/2).[33] The structures were solved by SHELXT (version 2018/2)[34] and refined by full-matrix least-squares procedures using

the Bruker SHELXTL (version 2018/3)[35] software package through the OLEX2 graphical interface.[36] All non-hydrogen atoms, including those in disordered parts, were refined anisotropically. Hydrogen atoms were included in idealized positions for structure factor calculations with $U_{iso}(H) = 1.2\ U_{eq}(C)$. More crystallographic and structure refinement details (Table S1) are shown in the Supporting Information.

Deposition Numbers 2219616 (for **3-u**), 2219616 (for **3-t**), 2219616 (for **8**), 2219616 (for **9**) contain the supplementary crystallographic data for this paper. These data are provided free of charge by the joint Cambridge Crystallographic Data Centre and Fachinformationszentrum Karlsruhe Access Structures service.

Calculations: Geometry optimizations were performed at the density functional theory level with the help (u)B97D3 based on Grimme's functional, which includes empirical dispersion.[37] All atoms including potassium were described by a triple-ζ basis set def2-TZVP.[38,39] Calculated structures were found to have a local minimum (no imaginary frequencies) on the corresponding potential energy surfaces, as determined by calculation of the full Hessian matrix, followed by estimation of frequencies in the harmonic approximation. Electronic energies include zero-point vibrational energy corrections. To elucidate the electronic structure of reduced *E*-**7**$^{2-}$ we carried out population, Mayer's bond order,[40] and natural bond orbital (NBO) analysis.[41] Visualization of the results were done with the GaussView 6 software. All calculations were performed with help of Gaussian Rev. C.01 software package.[42] The macrocyclic strain energy of conformer **3a** was calculated with the B97D3 method and the corresponding def2-TZVP basis set[38,39] using Gaussian code, via homodesmotic reactions (see the Supporting Information). More calculation details are shown in the Supporting Information.

Acknowledgements

T.A.S. gratefully acknowledges financial support by the German Research Council (DFG) and Fonds der chemischen Industrie (FCI). Financial support from the U. S. National Science Foundation, CHE-2003411, is gratefully acknowledged by M. A. P. Open Access funding enabled and organized by Projekt DEAL.

Conflict of Interest

The authors declare no conflict of interest.

Data Availability Statement

The data that support the findings of this study are available in the supplementary material of this article.

Keywords: alkali metals · chemical reduction · DFT calculations · macrocycle · reductive C–O cleavage · X-ray diffraction

[1] a) C. J. Pedersen, *J. Am. Chem. Soc.* **1967**, *89*, 2495; b) C. J. Pedersen, *J. Am. Chem. Soc.* **1967**, *89*, 7017.
[2] a) J. Yu, D. Qi, J. Li, *Commun. Chem.* **2020**, *3*, 189; b) Z. Liu, S. K. M. Nalluri, J. F. Stoddart, *Chem. Soc. Rev.* **2017**, *46*, 2459.
[3] M. Iyoda, J. Yamakawa, M. J. Rahman, *Angew. Chem. Int. Ed.* **2011**, *50*, 10522.
[4] a) Y. Segawa, K. Itami, A. Yagi, K. Matsui, *Angew. Chem. Int. Ed.* **2016**, *55*, 5136; b) D. Lu, Q. Huang, S. Wang, J. Wang, P. Huang, P. Du, *Front. Chem.* **2019**, *7*, 668; c) S. E. Lewis, *Chem. Soc. Rev.* **2015**, *44*, 2221.
[5] K. I. Assaf, W. M. Nau, *Chem. Soc. Rev.* **2015**, *44*, 394.
[6] a) V. Böhmer, *Angew. Chem. Int. Ed.* **1995**, *34*, 713; b) E. S. Español, M. M. Villamil, *Biomol. Eng.* **2019**, *9*.
[7] a) M. Xue, Y. Yang, X. Chi, Z. Zhang, F. Huang, *Acc. Chem. Res.* **2012**, *45*, 1294; b) J.-F. Chen, J.-D. Ding, T.-B. Wei, *Chem. Commun.* **2021**, *57*, 9029.
[8] a) W. Zhang, J. S. Moore, *Angew. Chem. Int. Ed.* **2006**, *45*, 4416; b) G. J. Bodwell, P. R. Nandaluru, *Isr. J. Chem.* **2012**, *52*, 105.
[9] a) D. T. Payne, W. A. Webre, Y. Matsushita, N. Zhu, Z. Futera, J. Labuta, W. Jevasuwan, N. Fukata, J. S. Fossey, F. D'Souza, K. Ariga, W. Schmitt, J. P. Hill, *Nat. Commun.* **2019**, *10*, 1007; b) H. Wu, Y. Chen, L. Zhang, O. Anamimoghadam, D. Shen, Z. Liu, K. Cai, C. Pezzato, C. L. Stern, Y. Liu, J. F. Stoddart, *J. Am. Chem. Soc.* **2019**, *141*, 1280; c) K. Kurihara, K. Yazaki, M. Akita, M. Yoshizawa, *Angew. Chem. Int. Ed.* **2017**, *56*, 11360; d) T. Iwamoto, Y. Watanabe, H. Takaya, T. Haino, N. Yasuda, S. Yamago, *Chem. Eur. J.* **2013**, *19*, 14061.
[10] T. Iwamoto, Y. Watanabe, T. Sadahiro, T. Haino, S. Yamago, *Angew. Chem. Int. Ed.* **2011**, *50*, 8342.
[11] a) A. Muñoz-Castro, *Phys. Chem. Chem. Phys.* **2018**, *20*, 3433; b) A. V. Zabula, A. S. Filatov, J. Xia, R. Jasti, M. A. Petrukhina, *Angew. Chem. Int. Ed.* **2013**, *52*, 5033; c) Z. Zhou, Z. Wei, T. A. Schaub, R. Jasti, M. A. Petrukhina, *Chem. Sci.* **2020**, *11*, 9395.
[12] A. Yu. Rogachev, Z. Zhou, S. Liu, Z. Wei, T. A. Schaub, R. Jasti, M. A. Petrukhina, *Chem. Sci.* **2021**, *12*, 6526.
[13] S. N. Spisak, Z. Wei, E. Darzi, R. Jasti, M. A. Petrukhina, *Chem. Commun.* **2018**, *54*, 7818.
[14] a) E. Kayahara, T. Kouyama, T. Kato, H. Takaya, N. Yasuda, S. Yamago, *Angew. Chem. Int. Ed.* **2013**, *52*, 13722; b) E. Kayahara, T. Kouyama, T. Kato, S. Yamago, *J. Am. Chem. Soc.* **2015**, *138*, 338.
[15] S. Taubert, D. Sundholm, F. Pichierri, *J. Org. Chem.* **2010**, *75*, 5867.
[16] S. Eder, D.-J. Yoo, W. Nogala, M. Pletzer, A. Santana Bonilla, A. J. P. White, K. E. Jelfs, M. Heeney, J. W. Choi, F. Glöcklhofer, *Angew. Chem. Int. Ed.* **2020**, *59*, 12958.
[17] a) M. Pletzer, F. Plasser, M. Rimmele, M. Heeney, F. Glöcklhofer, *Open Res. Europe* **2021**, *1*, 111; b) S. Eder, B. Ding, D. B. Thornton, D. Sammut, A. J. P. White, F. Plasser, I. E. L. Stephens, M. Heeney, S. Mezzavilla, F. Glöcklhofer, *Angew. Chem. Int. Ed.* **2022**, e202212623.
[18] a) K. M. Patel, R. J. Baltisberger, V. I. Stenberg, N. F. Woolsey, *J. Org. Chem.* **1982**, *47*, 4250; b) M. Lissel, J. Kottmann, *Z. Naturforsch.* **1988**, *43*, 11211; c) M. Itoh, S. Yoshida, T. Ando, N. Miyaura, *Chem. Lett.* **1976**, 271.
[19] S. Tanii, M. Arisawa, M. Yamaguchi, *Chem. Commun.* **2019**, *55*, 14078.
[20] H.-F. Grützmacher, A. Mehdizadeh, A. Mülverstedt, *Chem. Ber.* **1994**, *127*, 1163.
[21] M. T. Quick, M. Quick, I. N. Ioffe, C. Richter, R. Mahrwald, S. Druzhinin, S. A. Kovalenko, *J. Phys. Chem. B* **2020**, *124*, 1049.
[22] T. Fukushima, H. Sakamoto, K. Tanaka, Y. Hijikata, S. Irle, K. Itami, *Chem. Lett.* **2017**, *46*, 855.
[23] a) R. Kumar, A. Gaurav, S. Pal, K. R. Kumar, B. Sridhar, A. K. Tewari, *ChemistrySelect* **2017**, *2*, 3249; b) P. Kahl, J. P. Wagner, C. Balestrieri, J. Becker, H. Hausmann, G. J. Bodwell, P. R. Schreiner, *Angew. Chem. Int. Ed.* **2016**, *55*, 9277; c) B. Rezzonico, M. Grignon-Dubois, M. Laguerre, J.-M. Léger, *Organometallics* **1998**, *17*, 2656; d) A. Nangia, *Acc. Chem. Res.* **2008**, *41*, 595; e) A. J. Cruz-Cabeza, J. Bernstein, *Chem. Rev.* **2014**, *114*, 2170.
[24] M. Mirza-Aghayan, H. R. Darabi, L. Ali-Saraie, M. Ghassemzadeh, M. Bolourtchian, M. Jalali-Heravi, B. Neumüller, *Z. Anorg. Allg. Chem.* **2002**, *628*, 681.
[25] A. S. Filatov, N. J. Sumner, S. N. Spisak, A. V. Zabula, A. Yu. Rogachev, M. A. Petrukhina, *Chem. Eur. J.* **2012**, *18*, 15753.
[26] Y. Zhu, Z. Zhou, Z. Wei, M. A. Petrukhina, *Organometallics* **2020**, *39*, 4688.
[27] Z. Zhou, Z. Wei, K. Ikemoto, S. Sato, H. Isobe, M. A. Petrukhina, *Angew. Chem. Int. Ed.* **2021**, *60*, 11201.
[28] Z. Zhou, D. T. Egger, C. Hu, M. Pennachio, Z. Wei, R. K. Kawade, Ö. Üngör, R. Gershoni-Poranne, M. A. Petrukhina, I. V. Alabugin, *J. Am. Chem. Soc.* **2022**, *144*, 12321.
[29] a) H. Bock, K. Gharagozloo-Hubmann, M. Sievert, T. Prisner, Z. Havlas, *Nature* **2000**, *404*, 267; b) F. D. Romero, M. J. Pitcher, C. I. Hiley, G. F. S. Whitehead, S. Kar, A. Y. Ganin, D. Antypov, C. Collins, M. S. Dyer, G.

Klupp, R. H. Colman, K. Prassides, M. J. Rosseinsky, *Nat. Chem.* **2017**, *9*, 644; c) M. Pennachio, Z. Zhou, Z. Wei, S. Liu, A. Yu. Rogachev, M. A. Petrukhina, *Chem. Eur. J.* **2022**, *28*, e202104194.
[30] H. C. Wang, G. Levin, M. Szwarc, *J. Am. Chem. Soc.* **1977**, *99*, 2642.
[31] N. V. Kozhemyakina, J. Nuss, M. Jansen, *Z. Anorg. Allg. Chem.* **2009**, *635*, 1355.
[32] SAINT, part of Bruker APEX3 software package (version 2016.9-0), Bruker AXS, **2016**.
[33] SADABS, part of Bruker APEX3 software package (version 2016.9-0), Bruker AXS, **2016**.
[34] G. M. Sheldrick, *Acta Crystallogr. Sect. A* **2015**, *71*, 3.
[35] G. M. Sheldrick, *Acta Crystallogr. Sect. C* **2015**, *71*, 3.
[36] O. V. Dolomanov, L. J. Bourhis, R. J. Gildea, J. A. K. Howard, H. Puschmann, *J. Appl. Crystallogr.* **2009**, *42*, 339.
[37] S. Grimme, S. Ehrlich, L. Goerigk, *J. Comput. Chem.* **2011**, *32*, 1456.
[38] F. Weigend, R. Ahlrichs, *Phys. Chem. Chem. Phys.* **2005**, *7*, 3297.
[39] F. Weigend, *Phys. Chem. Chem. Phys.* **2006**, *8*, 1057.
[40] I. Mayer, *Chem. Phys. Lett.* **1983**, *97*, 270.
[41] a) K. H. Bowen, J. G. Eaton, R Naaman, *The Structure of Small Molecules and Ions*; Springer: New York, NY, **1988**; b) F. Weinhold, C. R. Landis, *Valency and Bonding. A Natural Bond Orbital Donor-Acceptor Perspective*, Cambridge University Press, Cambridge, UK, New York, **2005**.
[42] Gaussian 16, Revision C.01, M. J. Frisch, G. W. Trucks, H. B. Schlegel, G. E. Scuseria, M. A. Robb, J. R. Cheeseman, G. Scalmani, V. Barone, G. A. Petersson, H. Nakatsuji, X. Li, M. Caricato, A. V. Marenich, J. Bloino, B. G. Janesko, R. Gomperts, B. Mennucci, H. P. Hratchian, J. V. Ortiz, A. F. Izmaylov, J. L. Sonnenberg, D. Williams-Young, F. Ding, F. Lipparini, F. Egidi, J. Goings, B. Peng, A. Petrone, T. Henderson, D. Ranasinghe, V. G. Zakrzewski, J. Gao, N. Rega, G. Zheng, W. Liang, M. Hada, M. Ehara, K. Toyota, R. Fukuda, J. Hasegawa, M. Ishida, T. Nakajima, Y. Honda, O. Kitao, H. Nakai, T. Vreven, K. Throssell, J. A. Montgomery, Jr., J. E. Peralta, F. Ogliaro, M. J. Bearpark, J. J. Heyd, E. N. Brothers, K. N. Kudin, V. N. Staroverov, T. A. Keith, R. Kobayashi, J. Normand, K. Raghavachari, A. P. Rendell, J. C. Burant, S. S. Iyengar, J. Tomasi, M. Cossi, J. M. Millam, M. Klene, C. Adamo, R. Cammi, J. W. Ochterski, R. L. Martin, K. Morokuma, O. Farkas, J. B. Foresman, D. J. Fox, Gaussian, Inc., Wallingford CT, **2016**.

Manuscript received: February 22, 2023
Revised manuscript received: February 24, 2023
Accepted manuscript online: February 24, 2023